Research Article Vol. 1, No. 5 / 15 May 2022 / Optics Continuum 1003
OPTICS CONTINUUM

Extended Kalman filter and extended sliding innovation filter in terahertz spectral acquisition

Isaac Spotts,[1,4] C. Harrison Brodie,[1] Camille A. Leclerc,[1] S. Andrew Gadsden,[2] Mohammad Al-Shabi,[3] and Christopher M. Collier[1,5]

[1] *School of Engineering, The University of British Columbia, Kelowna, British Columbia, V1 V 1V7, Canada*
[2] *Department of Mechanical Engineering, McMaster University, Hamilton, Ontario L8S 4L8, Canada*
[3] *Department of Mechanical and Nuclear Engineering, The University of Sharjah, Sharjah, United Arab Emirates*
[4] *ispotts@ubc.ca*
[5] *Christopher.collier@ubc.ca*

Abstract: Terahertz spectral acquisition has a fundamental limitation in implementation due to long experimental acquisition time. The long experimental acquisition time in terahertz spectral acquisition is a result of the required high integration time associated with usable dynamic range signals acquired through delay stage interferometry. This work evaluates the effectiveness of a non-linear version of the Kalman Filter, known as the extended Kalman filter (EKF), and the recently developed extended sliding innovation filter (ESIF), for increasing dynamic range in terahertz spectral acquisition. The comparison establishes that the EKF and ESIF can reduce integration time (time constant) of terahertz spectral acquisition, with EKF reducing the integration time by a factor of 23.7 for high noise signals and 1.66 for low noise signals to achieve similar dynamic ranges. The EKF developed in this work is comparable to a nominal application of wavelet denoising, conventionally used in terahertz spectral acquisitions. The implementation of this filter addresses a fundamental limitation of terahertz spectral acquisition by reducing acquisition time for usable dynamic range spectra. Incorporating this real-time post-processing technique in existing terahertz implementations to improve dynamic range will permit the application of terahertz spectral acquisition on a wide array of time sensitive systems, such as terahertz reflection imaging, and terahertz microfluidics. This is the first implementation, to our knowledge, of Kalman filtering methods on terahertz spectral acquisition.

1. Introduction

Signal processing techniques for acquisition of spectral signals have become ubiquitous in the measurement of sensitive signals [1–3]. By using signal processing techniques, system design parameters can be less sensitive and instead rely on post processing data to achieve the same dynamic range (DR) [4,5]. To improve system DR, signal processing removes noise that is generated in the measurement process [6]. One conventional method to reducing noise generation in a measured system is to increase the integration time during the measurement process [7,8]. However, increasing scan duration will affect the feasibility of a system design to be introduced into industrial or commercial applications which require fast image scan times. Many optical technologies that have mechanical components such as interferometers or convolution-based detection can have limited applications due to high time constraints from the use of long time constant integration [9,10]. These optical systems can also have high noise due to their reliance on electrical components, which can output random gaussian noise [11–13]. Sliding innovation and Kalman filtering have recently been demonstrated as a signal processing technique that has been shown to reduce noise in optical systems with high noise, thereby reducing the integration time required for a similar signal quality [14–17].

#452661 https://doi.org/10.1364/OPTCON.452661
Journal © 2022 Received 30 Dec 2021; accepted 17 Mar 2022; published 25 Apr 2022

OPTICS CONTINUUM

An optical system that is sensitive to noise and therefore can particularly benefit from Kalman filtering is terahertz spectral acquisition. This sensitivity to noise is due to the low power of the signal and the large use of electrical components [1,7,9]. Terahertz spectral acquisition has been shown to be an effective optical tool in ground-breaking technologies such as early skin cancer detection, and gastrointestinal endoscopic diagnostics [18,19]. However, a flaw in using terahertz spectral acquisition, is the high experimentation time requirement caused by the mechanical convolution-based technique required for detection [9].

A common metric that is used to quantify noise in terahertz spectral acquisition is DR [20]. Many fields of Terahertz acquisition define DR using different methods of calculation [21]. In this work DR is defined as,

$$DR\ function = \frac{[Amplitude(frequency)]}{[mean(noise\ floor)]}. \tag{1}$$

The *noise floor* in this work, is defined as the integrated amplitude of the terahertz spectral acquisition frequency domain response between 6.5 to 8.3 THz for data sets, ensuring no bias is applied to any individual data set. The *noise floor* integrated frequency range strongly impacts the scaling applied to the DR. Thus, if the *noise floor* is changed between data sets, the scaling can appear to incorrectly increase the DR of a data set. The integrated frequency range values were chosen as the best fit for how the effect of time constant should theoretically affect DR, following the relationship provided by Vieweg *et al.* 2014 [7].

Applications with low peak dynamic range in terahertz spectral imaging are abundant due to the sensitivity of terahertz systems [22–24]. Recent advances in applications of terahertz detection such as terahertz microfluidics and, characterization of photoconductive antennas have suffered from low DR (as low as 6 dB) [25,26]. Alternatively, applications of terahertz spectral imaging such as terahertz reflection imaging are currently impeded by high measurement times [27,28]. Additionally, higher frequencies at the edge of the terahertz spectral image bandwidth will have a low DR. This low DR is caused by a decrease in amplitude as frequency approaches the upper range of the bandwidth [20,29]. The high frequencies of a terahertz spectral image contain extremely useful material information such as identifying chemical components [8]. Thus, increasing the DR is of vital importance to these applications to increase information retrieved from each spectral acquisition. To achieve acceptable DR in terahertz spectral acquisition applications, integration time is often increased and therefore imaging duration is also increased [7]. An integral improvement that must be accomplished before a viable application of terahertz spectral acquisition is achieved, is reduction of acquisition duration [30].

In this work we reduce the requirement of high integration times by using a recently developed extended sliding innovation filter (ESIF), and a non-linear version of the Kalman filter, the extended Kalman filter (EKF) [14]. The envisioned impact of this implementation is to help alleviate time constraints on impractical real-time applications of terahertz spectral imaging. A secondary goal of this work is to provide a comparison between these two filtering methods. Extending on the procedures in Gaamouri *et al.* 2018, these filters are compared to a Haar wavelet denoising method, and a nominal implementation of a tailored Daubechies (Db) wavelet denoising method [10]. A tertiary goal is to establish that EKF or the ESIF perform comparably or favorably to the wavelet denoising methods, as the Kalman and sliding innovation filtering methods can be implemented in real time [10,31]. The comparison is accomplished by taking several measurements at varying acquisition time constants. These measurements are then processed by each filter, whereby the system is modelled as two Gaussian functions, with alternating positive and negatives amplitudes, to approximate the bipolar THz waveforms seen in the time-domain.

OPTICS CONTINUUM

2. Terahertz spectral acquisition experimental parameters

In this section the parameters of each terahertz spectral acquisition scan, and the model used for the EKF are discussed. In Fig. 1 the terahertz spectral acquisition system used in the experimentation is depicted using a schematic. Eight terahertz spectral acquisition scans are produced using a gallium arsenide (GaAs) photoconductive THz antenna (i.e., Auston switch) for emission, and a ⟨110⟩ zinc telluride (ZnTe) crystal for electro-optic detection. Each terahertz spectral acquisition scan is conducted at a different acquisition time constant (τ) to provide a baseline for increasing integration time. The time constants used for the baseline are $\tau = 100$ µs, 300 µs, 1 ms, 3 ms, 10 ms, 30 ms, 100 ms, and 300 ms, and are recorded using a lock-in amplifier (Stanford Research Systems SR830). The time resolved time window of each scan is 15 ps (corresponding to 4.5 mm) with a step size of 0.05 ps (corresponding to 15 µm). Terahertz spectral acquisition scans are conducted in a non-Nitrogen purged environment, with ambient conditions such as vapor absorption lines observable in the scans.

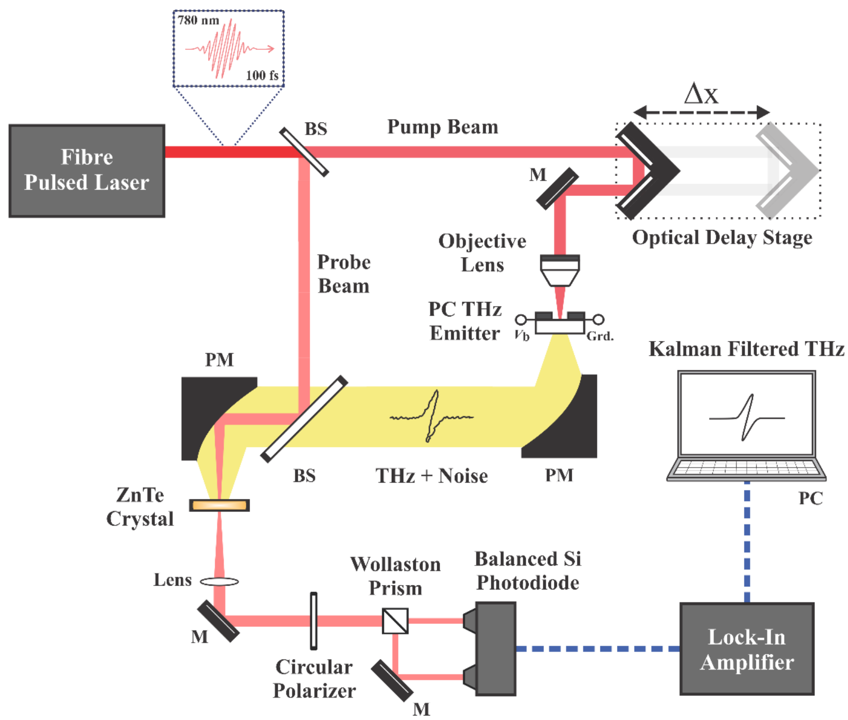

Fig. 1. A schematic of the terahertz time domain spectral acquisition set-up where BS is a beam splitter, M is a mirror, PC THz emitter is a photoconductive terahertz emitter, PC is a personal computer, PM is a parabolic mirror, and ZnTe crystal is a ⟨110⟩ Zinc telluride crystal.

3. Non-linear filter model parameters

To develop the model of the terahertz spectral acquisition scan, three gaussians are modeled to match the pulse shape. The EKF developed in this work follows the mathematical model that is provided in Spotts *et al*. 2020 [14]. The linearized model used in the EKF for the terahertz pulse

OPTICS CONTINUUM

is,

$$x_{k+1} = \begin{vmatrix} 1 & \mathrm{d}t \\ 0 & \Delta \end{vmatrix} x_k + w_k. \tag{2}$$

where x is the subscript k time domain data point, dt is the temporal spacing of the data set,

$$\Delta = \frac{3.88\, e^{\left(-\frac{5000\left[x-\frac{151}{50}\right]^2}{729}\right)}}{576} - \frac{1.17\, e^{\left(-\frac{25\left[x-\frac{87}{25}\right]^2}{2}\right)}}{144}. \tag{3}$$

and

$$w = \ \sim |Q|. \tag{4}$$

Here Q is the iteratively tuned model system noise covariance, which is provided below,

$$Q = \begin{vmatrix} 10^{-2} & 0 \\ 0 & 10^{-2} \end{vmatrix}. \tag{5}$$

The non-linear equation used in the EKF and the ESIF is

$$x_{k+1} = \begin{vmatrix} 1 & \mathrm{d}t(\dot{x}) \\ 0 & \Delta \end{vmatrix} x_k + w_k. \tag{6}$$

The iteratively tuned parameter representing measurement error covariance R is

$$R = \begin{vmatrix} 25 & 0 \\ 0 & 25 \end{vmatrix}. \tag{7}$$

The predictor-corrector model that the ESIF uses is different to the KF based model. The ESIF is a non-linear version of the sliding innovation filter. The ESIF uses a sliding mode approach to determine the true values of systems. To determine the gain of an ESIF filter Eq. (8) is used, being,

$$K_{k+1} = H^{+}_{k+1}\overline{sat}\left(\frac{|\tilde{z}_{k+1|k}|}{\delta}\right). \tag{8}$$

In Eq. (7) + denotes a pseudoinverse, $\overline{sat}$ denotes a diagonal matrix of elements that are equal to the saturated values, $|\tilde{z}_{k+1|k}|$ denotes the absolute innovation or measurement error within a system, and δ denotes a sliding boundary layer that is fundamental to the design of the filter and signal parameters. The sliding boundary layer is a tuneable parameter that has been iteratively optimised in this work to the values shown in (8) as

$$\delta = \begin{vmatrix} 2.5\times 10^{-3} & 0 \\ 0 & 1.1 \end{vmatrix}. \tag{9}$$

4. Dynamic range performance of non-linear filtering

In this section the performance of the EKF and the ESIF are evaluated and quantified by the increase in DR in comparison to an increase in time constant. For comparison the two extreme cases (low and high time constant) have been plotted in both the time domain and the frequency domain (DR function). In the time domain the jagged oscillation located before the terahertz

OPTICS CONTINUUM

pulse ($t\sim \leq 2.0$ ps) can be considered as noise in the terahertz spectral acquisition system. This noise propagates throughout the entire signal, however, after the terahertz pulse there is also the system response to the terahertz pulse (e.g., spectral features, etalon artifacts, etc.). The effect that the jagged oscillations have on signal quality can be quantified using the DR function. The DR of both the treated data and the untreated data at each time constant have been plotted to provide insight into any trend that may occur. The single DR value presented is determined by the integrated DR function in the frequency region between 0.2 and 1.0 THz. The average is taken to account for local maximas or minimas caused by the reflections in the electro-optic crystal detection terahertz detection method. These values are presented on a logarithmic scale, however the DR quoted is not in units of decibels.

In Fig. 2 the low time constant ($\tau = 100$ µs) is seen to have abundant jagged oscillations before the terahertz pulse occurs. A decrease in amplitude of the jagged oscillations located before the terahertz pulse occurs, is exhibited when the time constant is increased to $\tau = 300$ µs. The EKF visibly decreases the size of the jagged oscillations further than the increase in time constant when applied to the $\tau = 100$ µs data set. The EKF visibly has the highest reduction to the jagged oscillations prior to the terahertz pulse. The Haar and tailored Db wavelet denoising method follow a similar pattern to the ESIF and EKF, where the tailored Db decreases the jagged oscillations further than the Haar wavelet denoising method.

In Fig. 3, we examine the frequency response of the low time-constant case. The increase in time constant from $\tau = 100$ µs to $\tau = 300$ µs is shown to increase DR from $DR_{100\ \mu s}= 7.74$, to $DR_{300\ \mu s}= 12.0$. In Fig. 3(b) the Haar wavelet denoising method is seen have an incremental improvement to the DR ($DR_{Haar}= 80.9$), whereas the tailored Db implementation led to a drastic increase in DR ($DR_{Tailored\ Db}= 16.4$). Shown in Fig. 3(a) the $\tau = 100$ µs data set treated with the ESIF has an increase of $DR_{100\ \mu s}= 7.74$ to $DR_{ESIF}= 11.2$. The $\tau = 100$ µs data set treated with the EKF has the highest DR ($DR_{EKF}= 22.8$), which was more effective at increasing the DR than the increased time constant or the ESIF. The EKF increased the $\tau = 100$ µs data set DR by a factor of 2.95. This increase in DR verifies the noise reduction in the time domain response plotted in Fig. 2.

In Fig. 4, we examine a high time-constant case in the time-domain. The high time constant ($\tau = 100$ ms) is seen to have almost no visible jagged oscillations before the terahertz pulse occurs. When the time constant is increased to $\tau = 300$ ms there is no visible change to the signal in the time domain response. Additionally, when any filtering method is applied to the $\tau = 100$ ms data set there is no visible change to the signal in the time domain response.

In Fig. 5 the DR function of the high time constant data sets ($\tau = 100$ ms, $\tau = 300$ ms) indicate a comparable increase in DR when compared to the low time constant data sets ($DR_{100\ ms} = 72.6$, and $DR_{300\ ms} = 126$). The wavelet denoising methods manage to make an incremental improvement to the DR ($DR_{Haar}= 80.9$ and $DR_{Tailored\ Db} = 115$), lower than when applied to the high noise data sets seen in Figs. 2 and 3. For the high time constant case the ESIF performs similarly to the EKF ($DR_{ESIF}= 135$). The EKF has less of an increase in DR when treating high time constant data, with a DR close to the increased time constant data set ($DR_{EKF}= 130$). However, the EKF is still effective at increasing the DR with an increase in DR by a factor of 1.79.

In Fig. 6 we plot an exhaustive experimental analysis of the relationship between time constant and DR in terahertz spectral acquisition. This figure shows that at each corresponding time constant, the EKF will improve the DR greater than the increase in time constant, for the measured data set. However, as indicated by Figs. 2 and 4, there is a decrease in filter improvement over increasing integration time as the time constant increases. An experimental line of best fit is determined (i.e., highest R^2) to interpolate between time constant data points which produced an R^2 of 0.914. This experimental line of best fit was produced to determine the equivalent time constant required for the increase in DR due to the treatment of each filter.

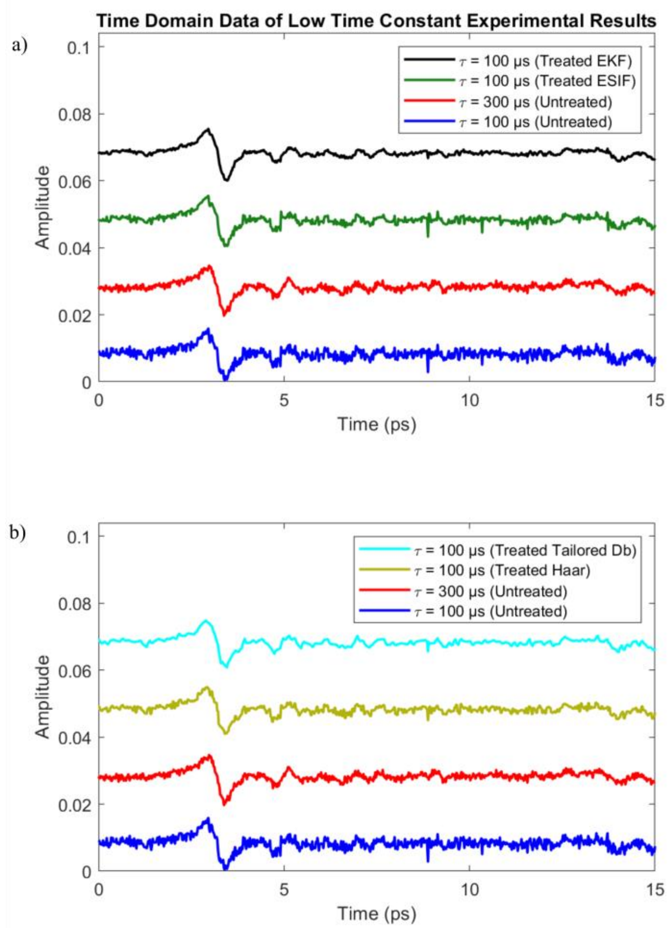

Fig. 2. The time domain of the $\tau = 100$ µs, $\tau = 300$ µs, and the treated $\tau = 100$ µs terahertz spectral acquisition data sets. The untreated $\tau = 100$ µs data set has been plotted with an (arbitrary) DC offset of 8.0×10^{-3} in both (a) and (b). The untreated $\tau = 300$ µs data set has been plotted with an (arbitrary) DC offset of 2.8×10^{-2} in both (a) and (b). The Haar (a), and the ESIF treated (b) $\tau = 100$ µs data set has been plotted with an (arbitrary) DC offset of 4.8×10^{-2}. The tailored Db (a), and the EKF (b) treated $\tau = 100$ µs data set have been plotted with an (arbitrary) DC offset of 6.8×10^{-2}. The DC offsets are solely for visualization purposes.

OPTICS CONTINUUM

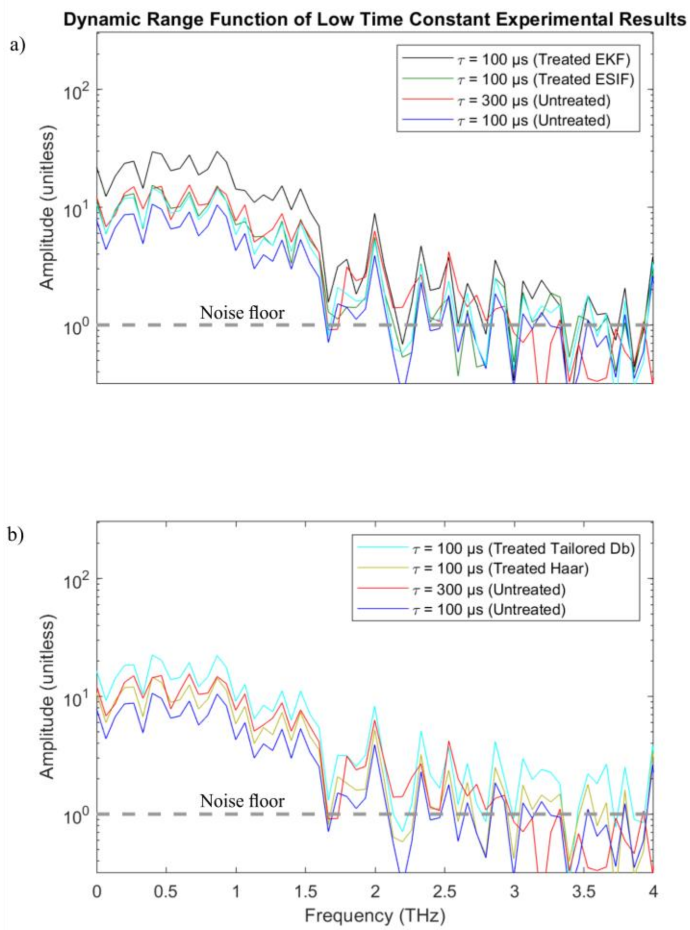

Fig. 3. The dynamic range function of the untreated $\tau = 100$ µs (DR = 7.74), untreated $\tau = 300$ µs (DR = 12.0), the ESIF treated $\tau = 100$ µs (DR = 11.2), and the EKF treated $\tau = 100$ µs (DR = 22.8) terahertz spectral acquisition data sets. In (b) the untreated data sets are compared to the Haar (DR = 10.6), and tailored Db (DR = 16.4) denoising methods.

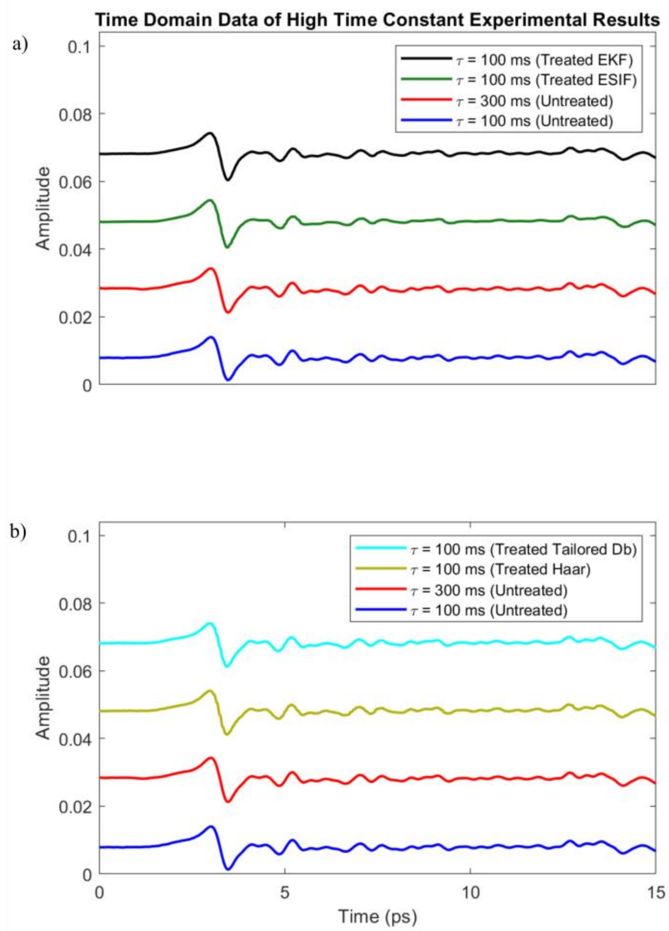

Fig. 4. The time domain of the $\tau = 100$ ms, $\tau = 300$ ms, and all treated $\tau = 100$ ms terahertz spectral acquisition data sets. The untreated $\tau = 100$ ms data set has been plotted with an (arbitrary) DC offset of 8.0×10^{-3} in both (a) and (b). The untreated $\tau = 300$ ms data set has been plotted with an (arbitrary) DC offset of 2.8×10^{-2} in both (a) and (b). The Haar (a), and the ESIF (b) treated $\tau = 100$ ms data set have been plotted with an (arbitrary) DC offset of 4.8×10^{-2}. The tailored Db (a), and the EKF (b) treated $\tau = 100$ ms data set have been plotted with an (arbitrary) DC offset of 6.8×10^{-2}. The DC offsets are solely for visualization purposes.

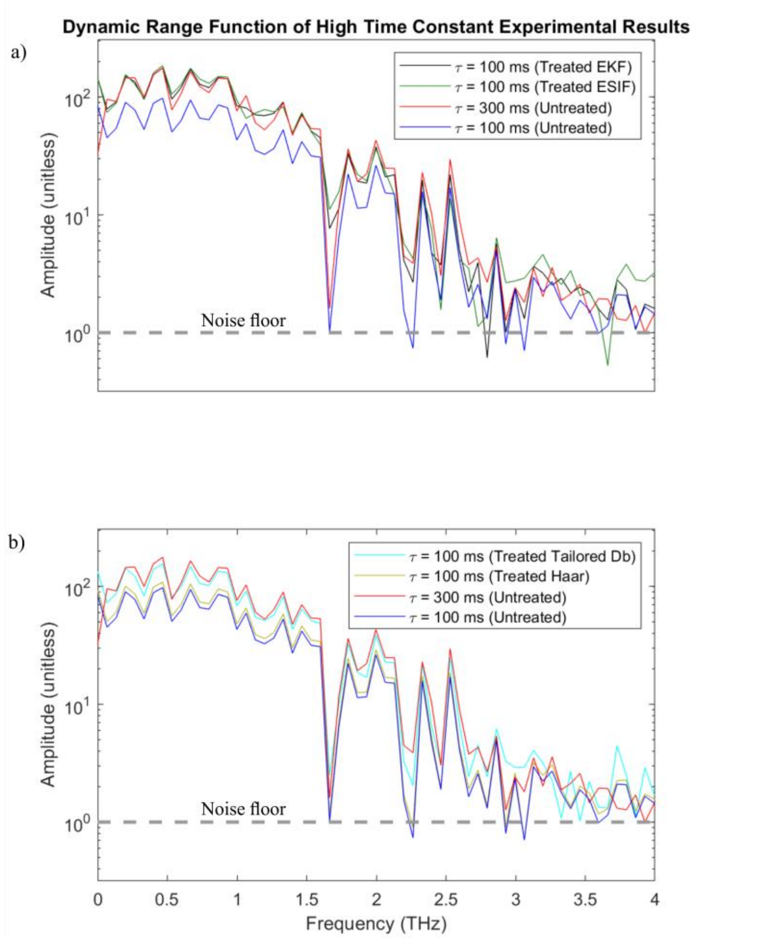

Fig. 5. In (a), the dynamic range function of the untreated $\tau = 100$ ms (DR = 72.6), untreated $\tau = 300$ ms (DR = 126), the ESIF treated $\tau = 100$ ms (DR = 135), and the EKF treated $\tau = 100$ ms (DR = 130) terahertz spectral acquisition data sets. In (b) the untreated data sets are compared to the Haar (DR = 80.9), and tailored Db (DR = 115) denoising methods. The high frequencies of the DR function are not centered around the *noise floor* because the range of frequencies chosen for the integration calculation remains constant between all data sets (6.5 to 8.3 THz).

OPTICS CONTINUUM

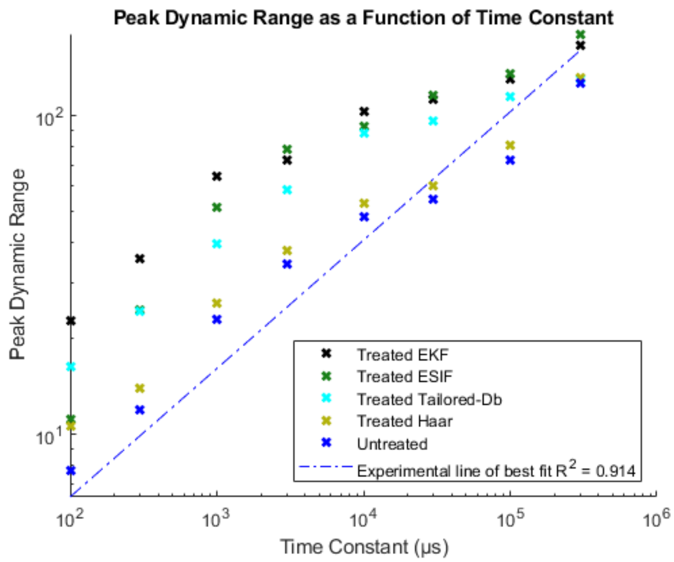

Fig. 6. The averaged peak dynamic range plotted as a function of time constant using all experimental terahertz spectral acquisition data sets (τ = 100 µs, 300 µs, 1 ms, 3 ms, 10 ms, 30 ms, 100 ms, and 300 ms), with an experimental line of best fit for the experimental data DR = $(\tau(\mu s))^{0.402}$.

To achieve an equivalent DR for the low time constant data set treated with the ESIF, following the experimental line of best fit, the time constant would need to be increased from $\tau = 100$ µs to 390 µs. To achieve an equivalent DR for the low time constant data treated with the EKF, following the experimental line of best fit, the time constant would need to be increased from $\tau = 100$ µs to 2.37 ms. This represents an improvement in image acquisition time of a factor of 23.7. For a 625 spatial pixel image (i.e., a 25 by 25 spatial pixel image), with the same 750 time increment scan as in our terahertz experiments, the overall imaging time would change from 19 minutes to less than one minute. To achieve an equivalent DR for the high time constant data set treated with ESIF, following the experimental line of best fit, the time constant would need to be increased from $\tau = 100$ ms to 182 ms. This represents an improvement in image acquisition time of a factor of 1.82. To achieve an equivalent DR for the high time constant data set treated with EKF, following the experimental line of best fit, the time constant would need to be increased from $\tau = 100$ ms to 166 ms. This represents an improvement in image acquisition time of a factor of 1.66. This indicates that the maximum DR improvement using the EKF occurs for terahertz spectral acquisition performed with a low time constant, resulting in a diminishing improvement for data sets acquired with a high time constant. The ESIF has a more consistent improvement on DR than the EKF, as the time constant is increased. Figure 6 also demonstrates that the implementation of the EKF is comparable to the tailored Db wavelet denoising method.

5. Dynamic range performance of non-linear filtering

In this paper, we introduced a novel application of EKF and the recently developed ESIF for treatment of terahertz spectral acquisition. The ESIF managed to increase dynamic range in the frequency domain, however, overall performed worse than the EKF. The EKF has the capability of improving the DR in terahertz spectral acquisition by approximately a factor of 2.95 increase at maximum and a factor of 1.79 increase at minimum for the presented data sets ($\tau = 100$ µs to

OPTICS CONTINUUM

$\tau = 300$ ms). Additionally, the EKF has shown to perform better than the Haar wavelet denoising method and is comparable to a nominal implementation of the tailored Db wavelet denoising method presented in the paper. Unlike the wavelet denoising methods, the EKF and ESIF also have the capability of filtering data sets in real-time. The time domain implementation of this filter has visibly shown a reduction in noise in the time domain, and drastically increased dynamic range in the frequency domain response. The implementation of these versatile filters can reduce experimentation times for a wide array of applications of terahertz spectral acquisition systems. Terahertz spectral acquisition is an innovative field that can revolutionize multiple fields of science. However, before implementation of terahertz spectral acquisition, fundamental limitations such as experimentation time must be addressed. This work presented a method to drastically reduce experimentation time (factor of 23.7) in terahertz spectral acquisition by reducing the required integration time for an equivalent DR. We believe these results have important implications for all terahertz imaging applications that require rapid scan times.

Funding. Natural Sciences and Engineering Research Council of Canada Discovery Grant Program (04022).

Disclosures. The authors declare no conflict of interest.

Data availability. Data underlying the results presented in this paper are not publicly available at this time but may be obtained from the authors upon reasonable request.

References

1. X. Zeng, Y. Liang, H. Zhang, X. Xi, J. Cao, B. Li, and J. Zhou, "Smoothing method to directly denoise terahertz signals in rare-earth orthoferrite antiferromagnets," J. Am. Ceram. Soc. **104**(7), 3325–3333 (2021).
2. E. G. Turitsyna and S. K. Turitsyn, "Digital signal processing based on inverse scattering transform," Opt. Lett. **38**(20), 4186 (2013).
3. T. Marshall, B. Szafraniec, and B. Nebendahl, "Kalman filter carrier and polarization-state tracking," Opt. Lett. **35**(13), 2203 (2010).
4. R. Al-Hujazy and C. M. Collier, "Design considerations for integration of terahertz time-domain spectroscopy in microfluidic platforms," Photonics **5**(1), 5–10 (2018).
5. N. Han, G. N. West, A. H. Atabaki, D. Burghoff, and R. J. Ram, "Compact and high-precision wavemeters using the Talbot effect and signal processing," Opt. Lett. **44**(17), 4187 (2019).
6. R. Peesapati, S. L. Sabat, K. P. Karthik, J. Nayak, and N. Giribabu, "Efficient hybrid Kalman filter for denoising fiber optic gyroscope signal," Optik (Munich, Ger.) **124**(20), 4549–4556 (2013).
7. N. Vieweg, F. Rettich, A. Deninger, H. Roehle, R. Dietz, T. Göbel, and M. Schell, "Terahertz-time domain spectrometer with 90 dB peak dynamic range," J. Infrared, Millimeter, Terahertz Waves **35**(10), 823–832 (2014).
8. J. Neu and C. A. Schmuttenmaer, "Tutorial: An introduction to terahertz time domain spectroscopy (THz-TDS)," J. Appl. Phys. **124**(23), 231101 (2018).
9. R. N. Alexander, N. C. Gabay, P. P. Rohde, and N. C. Menicucci, "Measurement-Based Linear Optics," Phys. Rev. Lett. **118**(11), 110503 (2017).
10. S. Gaamouri, M. B. Salah, and R. Hamdi, "Denoising ECG Signals by Using Extended Kalman Filter to Train Multi-Layer Perceptron Neural Network," Autom. Control Comput. Sci. **52**(6), 528–538 (2018).
11. M. Marzano, A. Cultrera, M. Ortolano, and L. Callegaro, "A correlation noise spectrometer for flicker noise measurement in graphene samples," Meas. Sci. Technol. **30**(3), 035102 (2019).
12. C. Harrison Brodie and C. M. Collier, "Single-point detection architecture via liquid crystal modulation for hyperspectral imaging systems," IEEE Access **8**, 185012–185020 (2020).
13. S. Z. S. Hassen, I. R. Petersen, C. K. Filtering, W. Bao, S. Member, X. Zhang, A. El-Keyi, T. Kirubarajan, A. B. Gershman, N. Zhang, A. Xu, K. Wang, X. Han, W. Hong, and S. H. Hong, "Remaining Useful Life Prediction of Lithium Batteries Based on Extended Kalman Particle Filter," IEEE Trans. Control Syst. Technol. **28**, 1143–1150 (2019).
14. I. Spotts, C. Harrison Brodie, S. Andrew Gadsden, M. Al-Shabi, and C. M. Collier, "Comparison of nonlinear filtering techniques for photonic systems with blackbody radiation," Appl. Opt. **59**(30), 9303 (2020).
15. G. R. Baez, J. A. Pomarico, and G. E. Elicabe, "An improved extended Kalman filter for diffuse optical tomography," Biomed. Phys. Eng. Express **3**(1), 015013 (2017).
16. A. El-Keyi, T. Kirubarajan, and A. B. Gershman, "Robust adaptive beamforming based on the Kalman filter," IEEE Trans. Signal Process. **53**(8), 3032–3041 (2005).
17. S. Z. S. Hassen and I. R. Petersen, "Frequency locking of an optical cavity using a time-varying kalman filtering approach," IEEE Trans. Contr. Syst. Technol. **22**(3), 1143–1150 (2014).
18. S. I. Hakeem and Z. A. Hassoun, "Skin Cancer Detection based on Terahertz Images by using Gabor filter and Artificial Neural network," IOP Conf. Ser.: Mater. Sci. Eng. **928**, 032025 (2020).
19. P. Doradla, C. Joseph, and R. H. Giles, "Terahertz endoscopic imaging for colorectal cancer detection: Current status and future perspectives," WJGE **9**(8), 346 (2017).

OPTICS CONTINUUM

20. P. U. Jepsen and B. M. Fischer, "Dynamic range in terahertz time-domain transmission and reflection spectroscopy," Opt. Lett. **30**(1), 29 (2005).
21. V. Skoromets, H. Němec, V. Goian, S. Kamba, and P. Kužel, "Performance Comparison of Time-Domain Terahertz, Multi-terahertz, and Fourier Transform Infrared Spectroscopies," J. Infrared, Millimeter, Terahertz Waves **39**(12), 1249–1263 (2018).
22. S. Takagi, S. Takahashi, K. Takeya, and S. R. Tripathi, "Influence of delay stage positioning error on signal-to-noise ratio, dynamic range, and bandwidth of terahertz time-domain spectroscopy," Appl. Opt. **59**(3), 841 (2020).
23. F. Bonnefoy, M. Bernier, E. Perret, N. Barbot, R. Siragusa, D. Hely, E. Kato, and F. Garet, "Video-rate identification of high-capacity low-cost tags in the terahertz domain," Sensors **21**(11), 3692 (2021).
24. R. I. Stantchev, X. Yu, T. Blu, and E. Pickwell-MacPherson, "Real-time terahertz imaging with a single-pixel detector," Nat. Commun. **11**(1), 2535 (2020).
25. S. Alfihed, I. G. Foulds, and J. F. Holzman, "Characteristics of Bow-Tie Antenna Structures for Semi-Insulating GaAs and InP Photoconductive Terahertz Emitters," Sensors **21**(9), 3131 (2021).
26. J. Xu, D. Liao, M. Gupta, Y. Zhu, S. Zhuang, R. Singh, and L. Chen, "Terahertz Microfluidic Sensing with Dual-Torus Toroidal Metasurfaces," Adv. Opt. Mater. **9**, 2100024 (2021).
27. S. N. Lowry, B. D. Price, I. D. Hartley, M. R. A. Shegelski, and M. Reid, "Reflection terahertz time-domain spectroscopy for imaging and identifying concealed interfaces in insulated systems," Appl. Opt. **60**(23), 6818–6828 (2021).
28. P. Kilcullen, M. Shegelski, M. Na, D. Purschke, F. Hegmann, and M. Reid, "Terahertz Spectroscopy and Brewster Angle Reflection Imaging of Acoustic Tiles," Journal of Spectroscopy **2017**, 1–6 (2017).
29. M. Naftaly, "Metrology Issues and Solutions in THz Time-Domain Spectroscopy: Noise, Errors, Calibration," IEEE Sens. J. **13**(1), 8–17 (2013).
30. E. Pickwell-MacPherson and V. P. Wallace, "Terahertz pulsed imaging-A potential medical imaging modality?" Photodiagn. Photodyn. Ther. **6**(2), 128–134 (2009).
31. T. Wu, W. Chen, E. Kerstel, E. Fertein, X. Gao, J. Koeth, K. Rößner, and D. Brückner, "Kalman filtering real-time measurements of H2O isotopologue ratios by laser absorption spectroscopy at 2.73 µm," Opt. Lett. **35**(5), 634–636 (2010).